Nuclear Instruments and Methods in Physics Research A 767 (2014) 310–317

Contents lists available at ScienceDirect

Nuclear Instruments and Methods in Physics Research A

journal homepage: www.elsevier.com/locate/nima

Dosimetric characterization of a synthetic single crystal diamond detector in a clinical 62 MeV ocular therapy proton beam

Marco Marinelli [a], F. Pompili [a], G. Prestopino [a,*], C. Verona [a], G. Verona-Rinati [a], G.A.P. Cirrone [b], G. Cuttone [b], R.M. La Rosa [b], L. Raffaele [b], F. Romano [b], C. Tuvè [c]

[a] INFN-Dipartimento di Ingegneria Industriale, Università di Roma "Tor Vergata", Via del Politecnico 1, I-00133 Roma, Italy
[b] Laboratori Nazionali del SUD, INFN, Catania, Italy
[c] INFN Sezione di Catania & Dipartimento di Fisica e Astronomia, Università di Catania, Catania, Italy

ARTICLE INFO

Article history:
Received 23 June 2014
Accepted 3 September 2014
Available online 16 September 2014

Keywords:
Synthetic diamond detector
Relative dosimetry
Proton therapy

ABSTRACT

A synthetic single crystal diamond based Schottky photodiode was tested at INFN-LNS on the proton beam line (62 MeV) dedicated to the radiation treatment of ocular disease. The diamond detector response was studied in terms of pre-irradiation dose, linearity with dose and dose rate, and angular dependence. Depth dose curves were measured for the 62 MeV pristine proton beam and for three unmodulated range-shifted proton beams; furthermore, the spread-out Bragg peak was measured for a modulated therapeutic proton beam. Beam parameters, recommended by the ICRU report 78, were evaluated to analyze depth-dose curves from diamond detector. Measured dose distributions were compared with the corresponding dose distributions acquired with reference plane-parallel ionization chambers. Field size dependence of the output factor (dose per monitor unit) in a therapeutic modulated proton beam was measured with the diamond detector over the range of ocular proton therapy collimator diameters (5–30 mm). Output factors measured with the diamond detector were compared to the ones by a Markus ionization chamber, a Scanditronix Hi-p Si stereotactic diode and a radiochromic EBT2 film. Signal stability within 0.5% was demonstrated for the diamond detector with no need of any pre-irradiation dose. Dose and dose rate dependence of the diamond response was measured: deviations from linearity resulted to be within $\pm 0.5\%$ over the investigated ranges of 0.5–40.0 Gy and 0.3–30.0 Gy/min respectively. Output factors from diamond detector measured with the smallest collimator (5 mm in diameter) showed a maximum deviation of about 3% with respect to the high resolution radiochromic EBT2 film. Depth-dose curves measured by diamond for unmodulated and modulated beams were in good agreement with those from the reference plane-parallel Markus chamber, with relative differences lower than $\pm 1\%$ in peak-to-plateau ratios, well within experimental uncertainties. A 2.5% variation in diamond detector response was observed in angular dependence measurements carried-out by varying the proton beam incidence angle in the polar direction. The dosimetric characterization of the tested synthetic single crystal diamond detector clearly indicates its suitability for relative dosimetry in ocular therapy proton beams, with no need of any correction factors accounting for dose rate and linear energy transfer dependence.

1. Introduction

Modern radiation therapy techniques are aimed to highly conform dose distribution to the target volume, sparing as much as possible healthy surrounding tissues and significantly reducing the possibility of side effects [1,2]. Most advanced treatments, such as Intensity Modulated Radiation Therapy (IMRT), are based on the delivery of high energy conformal photon beams from linear accelerators. High energy photons have the inherent disadvantage of scattering and delivering dose both proximal and distal to the target volume. The risk of radiation induced secondary cancers is therefore a serious issue [3].

As a result of an improved dose distribution [4,5] and of advances in delivery techniques [6,7], protons are gaining increasing interest worldwide as an elective treatment for specific types of tumors and the number of dedicated proton therapy facilities is rapidly growing [8]. The need of proton dosimetry standardization and of improvement of dosimetric accuracy have motivated the implementation of international dosimetry protocols [9,10], and a challenging optimization of detector technology. A comprehensive review on state-of-the-

* Corresponding author.
E-mail address: giuseppe.prestopino@uniroma2.it (G. Prestopino).

http://dx.doi.org/10.1016/j.nima.2014.09.004
0168-9002/

art detectors for measurement of absorbed-dose in clinical proton beams is reported in ICRU Report 78 [9] and Ref. [11].

Low-energy narrow proton beams (60–75 MeV) transported by using passive beam-delivery techniques have been employed, since the beginning of proton therapy, for the treatment of choroidal melanomas. Because of the small dimension of the proton eye treatment fields with associated sharp distal and lateral dose gradients, high resolution small volume detectors are required, with negligible linear energy transfer (LET) and dose rate dependence. For small field dosimetry international dosimetry protocols [9,10] recommend the use of detectors with a better spatial resolution compared to the standard plane-parallel ionization chambers.

Thanks to the high sensitivity per unit volume, small dimensions and high spatial resolution, solid state detectors such as silicon diodes and natural or first prototype synthetic diamond detectors have been reported as promising devices for relative proton dosimetry [9,11–17]. The attractive physical and dosimetric properties of diamond make it the material of choice for dosimetric applications. Nonetheless, the superiority of diamond based detectors for absorbed-dose measurement in proton beams has not yet been fully nor reproducibly demonstrated [14,16,17]. Major limitations pointed out for both silicon and state-of-the-art diamond detectors were significant LET, dose rate and energy dependence [9,11]. Such undesired effects were not observed in a novel synthetic diamond dosimeter recently reported in the literature by some of the authors of the present paper [18]. Moreover, contrary to diamond detectors, silicon diodes are also affected by a strong lattice radiation damage. A reduction in sensitivity of the order of tens percent after prolonged irradiation in low energy proton beams was reported [9,13,16,19].

Synthetic single crystal diamond technology offers the possibility to fabricate cost-effective and high performance detectors. Novel synthetic single crystal diamond detectors (SCDDs) grown by chemical vapor deposition (CVD) technique at the University of Rome “Tor Vergata” and designed as Schottky photodiodes have been successfully tested for radiotherapy dosimetry applications, in standard and small photon and electron beams [20–22].

In this paper the dosimetric performance of one such detector was tested in a proton beamline dedicated to the treatment of ocular diseases at the Laboratori Nazionali del Sud (LNS) of the National Institute of Nuclear Physics (INFN) in Catania, Italy. Detector response was investigated as function of dose, dose rate, LET and incidence direction of the radiation beam. Depth-dose distribution measurements were carried-out and compared to those from plane parallel chambers recommended by IAEA TRS-398 as reference detectors. Output factors were measured at reference depths (middle of the SOBP) and compared to those from other detectors commonly suggested for small beam dosimetry in clinical proton beams (Si-diodes and radiochromic films).

2. Materials and methods

2.1. Proton beam line

All measurements reported in this paper were performed at the proton beam line of the “Centro di AdroTerapia e Applicazioni Nucleari Avanzate” (CATANA) facility at INFN-LNS. A 62 MeV proton beam accelerated by a superconducting cyclotron is passively shaped and used for the treatment of ocular pathologies, like uveal melanoma and other less frequent lesions, such as choroidal haemangioma, conjunctiva melanoma, eyelid tumors, and embryonal sarcoma [23]. Fig. 1 shows a picture of the treatment room and a sketch of the proton beam line, with indication of the main transport elements [23,24]. The proton beam exits in air through a 50 μm kapton

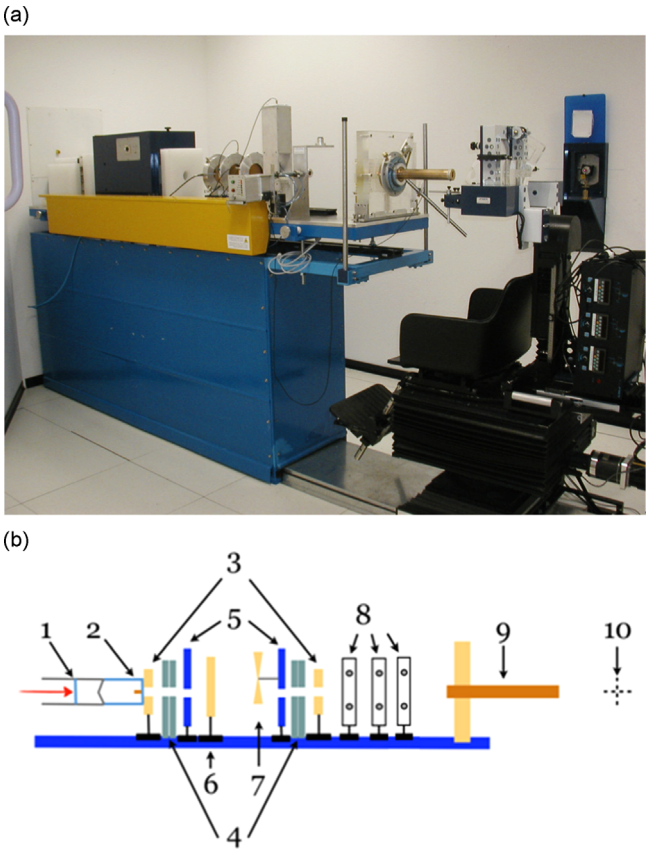

Fig. 1. (a) Photo of the CATANA treatment room. (b) Sketch of the proton delivery system and main beam line elements: (1) 1st scattering foil and SEM detector; (2) 2nd scattering foil with a central stopper; (3) plastic collimators; (4), (5) steel collimators; (6) range shifter; (7) modulator wheel; (8) monitor ionization chambers; (9) final collimator; and (10) isocentre.

window. Just before the exit window, in vacuum, a first 15 μm thick tantalum scattering foil is placed. In air, protons are transported for about 2.8 m before reaching the isocenter point, where calibration and measurements are performed. Different transport and diagnostic elements are placed along this path. The first element in air is a second tantalum foil, 25 μm tick, provided with a central brass stopper of 4 mm in diameter. The two-foils scattering system is designed to broaden the beam in order to provide a uniform lateral off-axis dose distribution at the irradiation point, while minimizing energy loss. Moreover, the first 15 μm tick tantalum scattering foil is employed as a Secondary Electron Monitor (SEM), and its voltage signal V_{sf} provides a real-time measurement of the beam intensity and, by means of an empirical formula, gives an estimation of the actual dose-rate. The SEM response is linear for the proton beam currents used for the measurements described in the present work, which also correspond to the rates typically used for treatments.

The range shifter (RS) and the range modulator (RM), placed downstream of the scattering system, are used respectively to change and to modulate the beam energy. In particular, the last one allows to obtain a spread-out Bragg peak (SOBP) longitudinally overlapped with the treatment volume. The RS consists of 17×17 cm^2 square PolyMethylMethacrylate (PMMA) slabs of different thicknesses, which are combined to achieve a total thickness in the range between 0.5 and 18.0 mm in steps of 0.2 mm. The RM is a PMMA wheel rotating at a fast constant speed and split in several angular sectors of increasing thickness: protons crossing the largest (smallest) thickness match the proximal (distal) edge of the SOBP. Downstream of the RM, two transmission monitor parallel plate ionization chambers provide the on-

line monitor of the dose delivered to the patient. Delivered dose is recorded in terms of monitor units by using the two monitor chambers calibrated with respect to a parallel plate Markus ionization chamber (PTW type 23343) according to the IAEA TRS 398 protocol [10]. A detailed description of the dosimetric procedures adopted at the CATANA irradiation beam line can be found in Ref. [25]. Following the monitor chambers, a 370 mm long brass collimator with an internal diameter of 36 mm is used to limit the beam angular spread. A further patient customized collimator, whose aperture matches the planned target volume, is inserted at the output of the brass collimator, in order to conform the proton beam according to the tumor target shape. Unless otherwise specified, a 25 mm in diameter reference collimator was used for the current experiments. Finally, a system based on laser sources is used to provide the isocenter identification, placed 83 mm far from the final collimator, where all the measurements described in this work have been carried out.

2.2. Detectors and measurement setup

The synthetic SCDD studied in the present work was based on a similar design of a SCDD investigated in a previous paper [20]. Details on device technology, detection mechanism, encapsulation technique and geometrical specifications can be found elsewhere [20,26]. Briefly, the device acts as a Schottky barrier photodiode and was operated in photovoltaic mode, i.e. at zero bias voltage. A leakage current of about 20 fA was found at room temperature for the studied SCDD. The detector sensitive volume is about 0.0038 mm^3, approximately defined by a cylindrical volume 2.2 mm in diameter and $\sim$1 μm thick. The diamond plate was embedded in a PMMA waterproof cylindrical housing, 8 mm in external diameter and 35 cm long, filled by epoxy resin, and connected to a low noise triaxial cable/connector. The reference measurement point for SCDD was therefore assumed to be at the center of the top diamond surface, located 1.5 mm below the top surface of the PMMA housing. In the present study the SCDD was tested, unless otherwise specified, with its long axis parallel to the beam direction. The SCDD was connected through a 20 m triaxial cable to a PTW Unidos Electrometer for charge measurements, or to a standard *I*/*V* acquisition board for depth-dose measurements and dose rate dependence measurements.

According to IAEA protocol TRS-398 [10], a PTW Markus plane-parallel ionization chamber, model 23343 (MK-IC in the following), was used for reference dosimetry of proton beam. The collecting electrode diameter is 5.3 mm, with an electrode spacing of 2 mm and a polarizing voltage of 300 V. The PTW Advanced Markus plane-parallel ionization chamber, model 34045 (AMK-IC in the following), was used as the reference detector for depth-dose measurements of both unmodulated and modulated proton beams. The Advanced Markus chamber is a perturbation-free version of the classic Markus chamber, because of a larger guard ring width (2 mm) and a smaller electrode spacing (1 mm), the latter assuring higher spatial resolution than conventional Markus chamber. The high electrical field strength (4000 V cm^{-1}) provides a collection efficiency close to unity up to 100 Gy/min in the continuous proton beam produced with the superconducting cyclotron. For in water measurements plane-parallel chambers were supplied with a waterproof 0.87 mm thick PMMA cap, screwed onto the chamber until lines of the cup and the chamber body match each other.

A PTW Unidos Electrometer was used for all charge measurements with plane-parallel chambers.

A dedicated eyeline water phantom, made in-house according to the IAEA TRS-398 protocol [10], was used in our investigations. The phantom consists of a PMMA cubic tank ($20 \times 20 \times 20$ cm^3), with a PMMA circular window 80 mm in diameter and 1.5 mm thick, through which the proton beam was incident. The phantom is provided of a computer-controlled motorized system, with a maximum scanning resolution along proton beam axis up to 0.1 mm. The acquisition software, developed at INFN-LNS, controls detector movements, providing also dosimetric analysis of acquired data. Tested and reference detectors were placed one at a time in the water phantom by using specific PMMA holders connected to a high precision motorized system; depth uncertainty was quoted as 0.1 mm.

The minimum depths achievable in the water phantom were 3.6 mm for SCDD and 2.8 mm for Markus chamber, which corresponded to the sum of the water-equivalent thicknesses of all material layers in front of the effective points of measurements. According to IAEA TRS 398 protocol [10], a depth scaling factor of 0.974 was used to convert depths in PMMA to equivalent depths in water. The calculated water equivalent depths of both detectors were accounted for in the computerized automatic scanning/positioning system.

Output factors (OFs) measurements in small proton beams were performed by using the SCDD, a Scanditronix Hi-p Si Photon Field Detector (PFD) diode, radiochromic EBT2 films and the Markus chamber. The dosimetric properties in clinical low energy proton beams of PFD diode and EBT2 films are well documented [12,27].

2.3. Measurement details

The dosimetric characteristics of the SCDD were investigated in the proton beams of the CATANA facility in terms of pre-irradiation dose, linearity with dose, dose rate dependence and angular dependence; also the accuracy of the SCDD in the depth-dose curves reconstruction, of both unmodulated and modulated proton beams, was tested. Finally field size factors for the smaller beams were experimentally evaluated.

Pre-irradiation, dose and dose rate dependence were investigated in the full energy proton beam by placing the SCDD at the minimum water-equivalent depth achievable. This corresponded, also taking into account the water phantom entrance window thickness, to 3.6 mm in water.

The pre-irradiation procedure for the SCDD was carried out by delivering a total dose of 24 Gy, in 12 fractions 2 Gy each. After each fraction, the charge M_{SCDD} from diamond and the actual delivered dose, as provided by the two calibrated transmission ion chambers according to the daily calibration data, were recorded.

Linearity with dose measurement was performed in the 0.5–40 Gy range. Three independent charge measurements (M_{SCDD}) were recorded at each step, i.e. for the same nominal delivered dose.

Dose rate dependence of the SCDD response was investigated by varying the proton beam current. The diamond detector current was sampled at 30 Hz, and the associated proton beam current from the 15 μm tick tantalum SEM scattering foil (see Section 2.1) was simultaneously recorded. Both diamond and SEM currents were converted into voltage signals, by means of two independent current–voltage converters. A standard acquisition board, operating in the $\pm$10 V range, was used for the acquisition. The SEM voltage signal allowed the normalization of the SCDD response against beam current fluctuations. Moreover, the voltage signal from the SEM scattering foil (V_{sf}) provided the actual dose rate by applying an empirical conversion formula: DR(Gy/min)$=28.94V_{sf}-0.2945$. Variations in beam current resulted in dose rate variations in the 0.33–30 Gy/min range.

Proton dose calibrations (determination of the factor cGy/MU) were carried out with the MK chamber in the water phantom for a 25 mm diameter circular collimator, stated as the reference collimator for the dosimetry of the proton eyeline. Proton dose calibrations of the unmodulated proton beams were carried out at a depth of 3.6 mm in the entrance region of the Bragg curve, representing the

minimum measurement depth achievable in the water phantom for the SCDD in the horizontal proton beam line. For modulated beams dose calibration was performed at a depth in water phantom corresponding to the middle of SOBP ($z_{ref.}$). According to IAEA-398 protocol, overall accuracy of dose measurements resulted to be about $\pm 3\%$ [10]. The SCDD calibration (nC/Gy) was assessed in the water tank by comparison with the reference MK chamber, as for unmodulated and modulated proton beams.

Central-axis depth dose measurements were performed with the SCDD and the AMK-IC. The detectors were placed, one at a time, on their respective holders inside the water phantom and connected to the remotely controlled motorized system. Five depth-dose curves (DDCs) were acquired: the one corresponding to the 62 MeV full energy proton beam, three range-shifted proton beams, and one therapeutic modulated proton beam. Depth-dose distributions for unmodulated and modulated proton beams were measured with the 25 mm diameter reference circular collimator; a distance of 8.5 cm was chosen between the final collimator and the front surface of the phantom and it was maintained fixed for all measurements. Measured DDCs from SCDD and AMK-IC were quantitatively evaluated by means of comparative analysis, and using the DDC parameters recommended by dosimetry protocols [9,10].

Output factors (cGy/MU) were determined with different detectors for collimator areas encountered in clinical practice, corresponding to collimator diameters in the range of 5–30 mm; the results were normalized to unity for the 25 mm diameter circular collimator (reference collimator). OFs were calculated as the ratio of detector readings at the measurement depth for the investigated collimator [$L(\phi)$] and the reference collimator [$L(\phi_0)$] used for standard proton beam calibration; detector readings were taken for the same monitor unit setting, calculated to deliver a dose of 5 Gy with the reference collimator.

The characteristics of the investigated detectors are summarized in Table 1. Markus plane-parallel ion chamber, PFD Si diode and SCDD detector were irradiated in the water phantom at a water equivalent depth of 14 mm, corresponding to the middle ($z_{ref.}$) of a 21 mm SOBP, representing a realistic ocular proton therapy situation; EBT2 films were irradiated at the same depth in a solid water slab phantom (PTW RW3). PFD diode and SCDD detector were irradiated with detector stems parallel to the proton beam axis, while the Markus chamber and EBT2 films were irradiated normally to the beam axis. EBT2 film was taken as the reference detector for OF measurements; exposed EBT2 film sheets ($6 \times 6\ cm^2$) were digitized 24 h after irradiation using an Epson 10000XL RGB Epson scanner and analyzed with Mephysto mc^2 PTW dosimetry software.

The effect of field size in output (beam dose/MU) has to be carefully determined because of the small dimensions of narrow proton beams employed in ocular proton therapy (40–500 mm^2); the change of collimator area can indeed result in a significant variation of output factor related principally to collimator edge scattering.

The angular dependence of the SCDD was investigated in air, with the diamond detector placed in a sample holder capable of rotating around its axis. Polar angular dependence was evaluated, with the detector long axis tilted with respect to the proton beam direction. A goniometer was used in order to rotate the SCDD by steps of 5° each and with a precision of 0.1°. The same SOBP used for output factor measurements was used, and five irradiations, ~5 Gy each, were performed at each angle.

Table 1
Sensitivity and relevant constructive features of detectors used for OF measurements.

Detector	Sensitivity (nC/Gy)	Active size[a] and sensitive volume
SCDD	1.11	Ø 2.2 mm 0.0038 mm^3
MK-IC	1.82	Ø 5.3 mm 55 mm^3
PFD Si	1.25	Ø 0.6 mm 0.017 mm^3
EBT2	–	0.08 mm/pixel

[a] Active size indicates the dimension of the sensitive volume facing the impinging proton beam. For the EBT2 the scanning resolution is reported.

3. Results and discussion

3.1. Pre-irradiation procedure, dose and dose rate dependence

The pre-irradiation procedure for the tested SCDD is shown in Fig. 2. Charge readings are normalized to the first recorded value, measured after the first 2 Gy irradiation step. A percentage variation within 0.5% can be observed in the whole pre-irradiation process, with a signal stability of ~0.2% (1σ) after about 6 Gy. Such short-term stability of SCDD response was observed to be maintained also during daily use, with no need of further pre-irradiation.

Such a priming-less behavior is completely different from what was reported for commercial natural or prototype synthetic diamonds under ionizing radiation [15,17,28,29]. The observed behavior indicates a low defect content in the sample, which can be ascribed both to the extremely thin active volume and to the high quality diamond of the fabricated SCDD.

The linearity of SCDD response with dose is shown in Fig. 3(a) up to 40 Gy, where the charge measured by the SCDD with respect to the delivered dose and the correspondent linear fit are plotted. The R^2 parameter of the linear best fit resulted to be one with a precision of 10^{-5}. A sensitivity of 1.11 nC/Gy was derived from the slope of the linear fit of the measured data. The stability with dose of the SCDD sensitivity, i.e. the M_{SCDD} to the delivered dose ratio, is reported in Fig. 3(b) as the percentage deviation with respect to the value at the maximum delivered dose. Deviations within 0.5% can be observed in the whole evaluated dose range, well within the experimental error.

The dose rate (DR) dependence analysis of the SCDD response is shown in Fig. 4. The voltage signal form the SCDD, which is proportional to the SCDD current, is shown in Fig. 4(a) as function

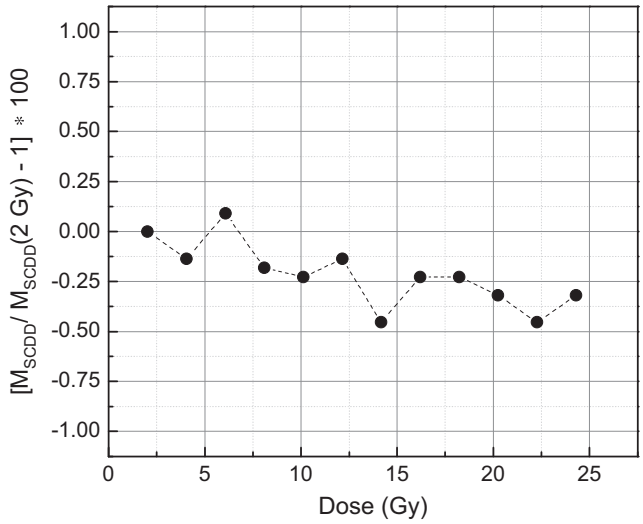

Fig. 2. Pre-irradiation procedure of the SCDD. Charge readings from the SCDD are reported vs. delivered dose as percentage deviation with respect to the first measured value.

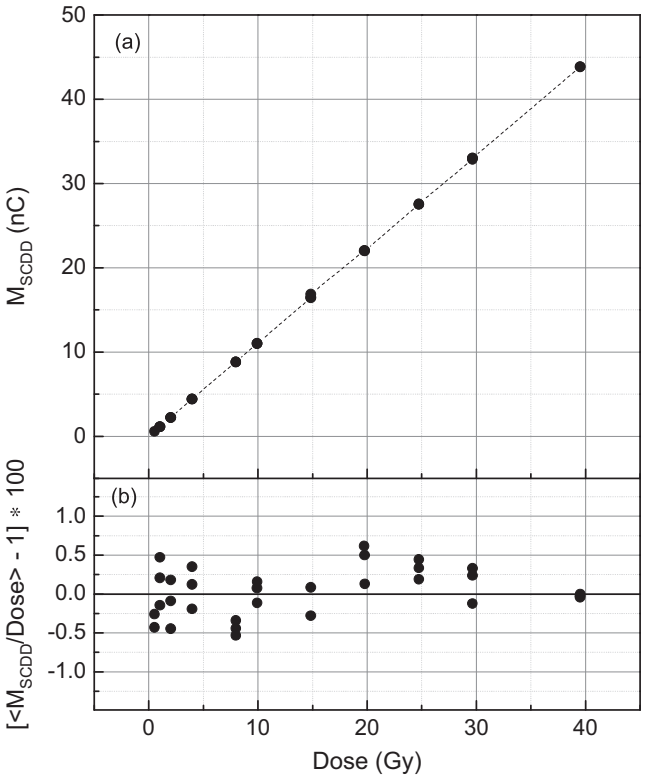

Fig. 3. (a) Charge measured by SCDD as function of proton delivered dose at the entrance of the full energy CATANA proton beam. (b) Percentage deviation of the measured charge to delivered dose ratio normalized at the maximum dose.

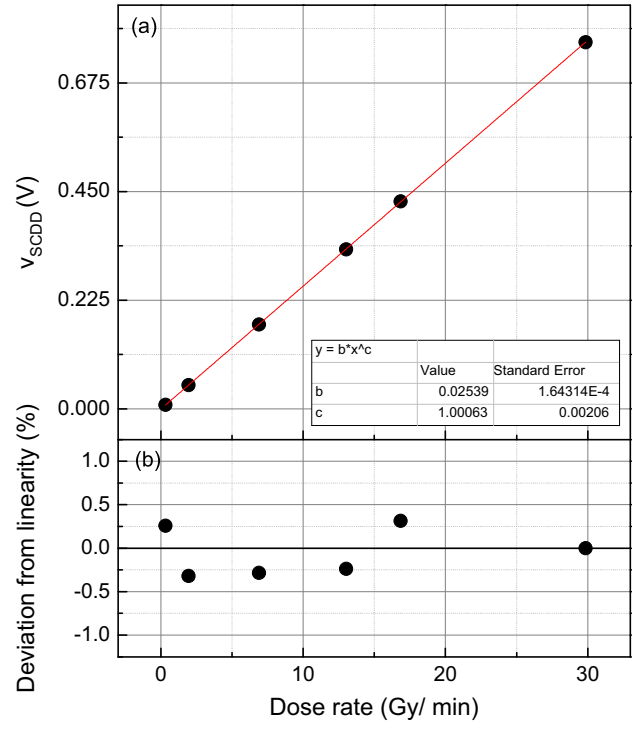

Fig. 4. (a) SCDD response as a function of the proton beam dose rate, extrapolated by the SEM voltage signal V_{sf} (DR(Gy/min)=28.94V_{sf} −0.2945). (b) Percentage deviation from linearity.

of the proton beam dose rate extrapolated by the SEM voltage signal V_{sf}. Data are fitted according to Flower's formula $I=\alpha\dot{D}^{\Delta}$ [30], where I is the detector current corrected for the dark current, α is a constant, $\dot{D}$ is the dose rate and Δ is a correction term accounting for an eventual dose rate dependency. For the tested SCDD a Δ value of 1.000 ± 0.002 was found, implying that the SCDD response is dose rate independent and no correction factors have to be applied. Such favorable behavior is not observed for state-of-the-art diamond detectors and silicon detectors, in which case Δ values of ~0.990 [13,14,16] and 1.021 [14] are reported, respectively. As reported in Fig. 4(b), a deviation from linearity below $\pm0.5\%$ was found, well within experimental uncertainties, confirming the negligible dose rate dependence of the tested SCDD.

It is worth to point out that the obtained results related to the pre-irradiation, linearity with dose and dose rate dependence measurements with the tested SCDD are fully consistent with the ones previously reported for similar SCDDs tested in clinical photon and electron beams [20,21], indicating that device performance is not dependent on radiation quality.

3.2. Depth-dose curves

Fig. 5(a) shows central axis depth-dose distributions as measured with the SCDD and the reference Advanced Markus plane-parallel IC, which refer to the full-energy proton beam and three different range-shifted proton beams; the curves are normalized to the signal at 4.4 mm depth in the entrance region of the Bragg curve. Difference plot between the depth-dose curves measured by the SCDD and the AMK-IC for the full-energy proton beam is also provided.

Fig. 5(b) shows the central axis depth-dose distribution of a modulated proton beam as measured by the SCDD and the AMK-IC; for modulated beams data were normalized at the depth of penetration at full dose d_{100} (27.7 mm), according to the ICRU Report no. 78 [9]. As for unmodulated proton beams, the difference plot between is provided.

An excellent agreement between depth dose curves measured by SCDD and plane-parallel chamber is clearly observed for unmodulated and modulated proton beams. A quantitative analysis of the measured DDCs is provided in Table 2, in terms of the parameters recommended by the ICRU Report no. 78 [9]: (i) depth of penetration (d'_{90}) for unmodulated beams, (ii) SOBP length (m'_{90}) for modulated beams, (iii) distal-dose falloff distances $DDF_{(90-10\%)}$ and $DDF_{(80-20\%)}$ and (iiii) peak-to-plateau ratios for the unmodulated proton beams.

Negligible differences, within experimental uncertainties, related to detector positioning and determination of effective point of measurements, can be observed in the computed parameters reported in Table 2. Values of the peak-to-plateau ratios measured by SCDD and Advanced Markus IC were found to agree to $\pm1\%$. Such small deviations indicate that the SCDD response is not affected by the LET values in the investigated energy range. This result is markedly different from the ones reported in literature for state-of-the art dosimeters based on solid state detectors [12–14,16,17] as well as radiochromic films [31], which are found to significantly over-/under-estimate the Bragg peak.

As discussed in Section 3.1, the SCDD favorable behavior in terms of LET dependence could be attributed to the extremely thin and high quality sensitive volume of the investigated device. Work is in progress to better clarify such LET independent behavior.

3.3. Output factors

Fig. 6(a) shows the measured OFs (cGy/MU) as a function of the collimator diameter. The different trends of the experimental OFs for MK-IC, Si PFD diode and SCDD can be ascribed to the differences in detector sensitive volumes (see Table 1), and to different volume averaging effects due to scattered radiation as the collimator diameter decreases. In Fig. 6(b) the percentage differences of OFs from SCDD, MK-IC and PFD Si diode with respect to the ones from reference EBT2 films are reported. In the case of

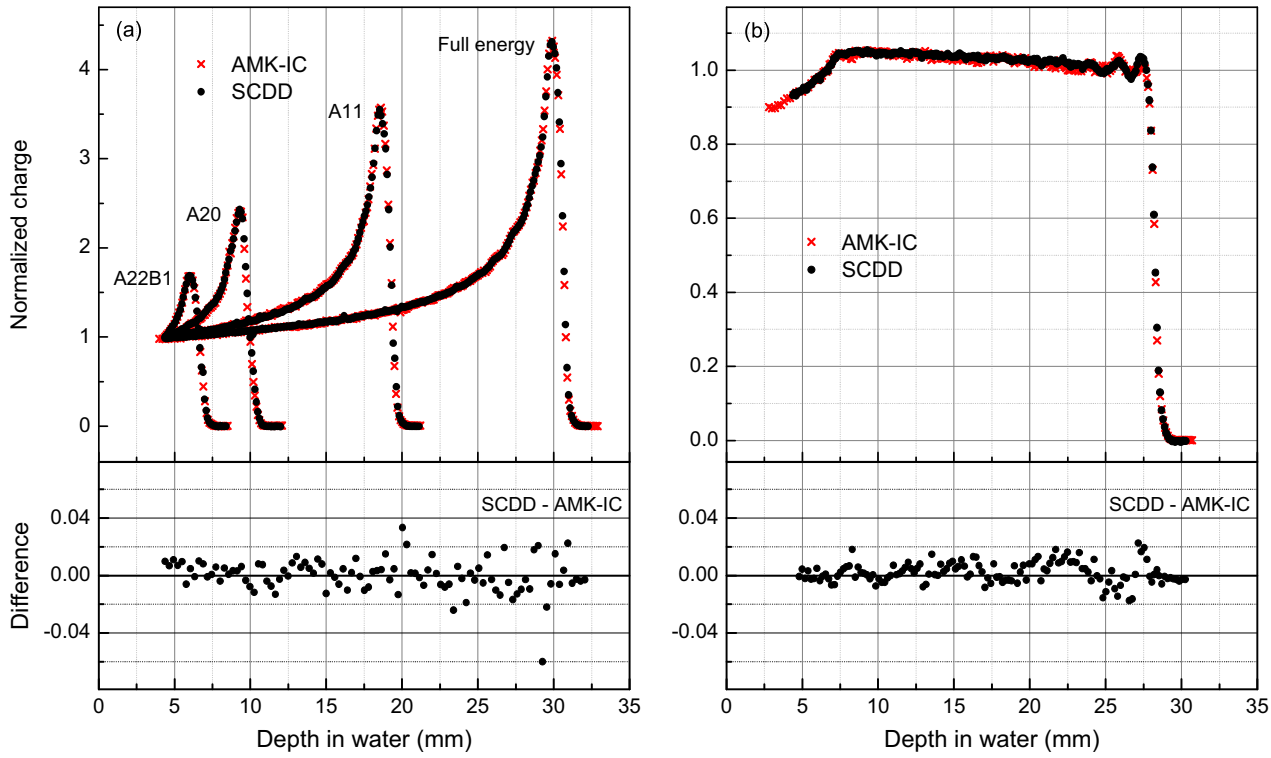

Fig. 5. (a) Central-axis depth dose curves measured by the SCDD and the AMK-IC for the unmodulated Bragg peaks and difference plot between SCDD and AMK-IC curves for the full energy (62 MeV) proton beam. (b) Depth dose curves and difference plot for the SCDD and the AMK-IC in the modulated proton beam.

Table 2
PDD analysis parameters for depth dose curves reported in Fig. 5 (a) and (b).

Proton Beam	d'_{90}, m'_{90} (mm)[a]			$DDF_{(90-10\%)}$ (mm)			$DDF_{(80-20\%)}$ (mm)			Peak-to-plateau ratio		
	SCDD	AMK-IC	diff.	SCDD	AMK-IC	diff.	SCDD	AMK-IC	diff.	SCDD	AMK-IC	diff. (%)[b]
F.E. 62 MeV	30.2	30.2	0.0	0.7	0.7	0.0	0.5	0.5	0.0	4.320	4.324	−0.1
11.5[c]	18.9	18.9	0.0	0.8	0.7	0.1	0.5	0.5	0.0	3.547	3.574	−0.7
21[c]	9.5	9.5	0.0	0.9	0.8	0.1	0.6	0.6	0.0	2.430	2.417	0.5
24[c]	6.3	6.3	0.0	0.8	0.8	0.0	0.5	0.5	0.0	1.693	1.693	0.0
SOBP	24.7	24.7	0.0	0.7	0.7	0.0	0.4	0.4	0.0	–	–	–

[a] The quantities d'_{90} and m'_{90} refer to the unmodulated distal 90% and to the SOBP length, respectively.
[b] Percentage difference of peak-to-plateau ratio of SCDD with respect to that from AMK-IC.
[c] Range shifter thickness (mm water-equivalent).

SCDD a maximum deviation of 3% can be noticed when using the 5 mm collimator. In particular, assuming a 2% deviation from reference OFs measured by EBT2 films as a reasonable threshold, Markus chamber can be used with collimators not smaller than about 13 mm in diameter, whereas SCDD and Hi-p Si diode allow reliable OF measurements down to about 8 mm.

The result found for the MK-IC agrees with IAEA TRS 398 recommendations for the use of plane parallel ICs in small proton beams [10], according to which detectors with better spatial resolution have to be used if the irradiation field size is smaller than twice the diameter of the IC sensitive volume.

Moreover, it must be pointed out that collimators with diameters smaller than 8 mm represent no more than 10% of all clinical eye treatment portals. The proposed SCDD could, therefore, provide a less time consuming alternative to EBT2 films for an accurate dosimetry of narrow ocular proton beams.

3.4. Angular dependence

The angular dependence of the SCDD response is shown in Fig. 7. Measured data are reported as percentage deviation of the detector sensitivity (nC/Gy) from its response at 0°. An overall deviation of 2.5% was found in the 0° to ±90° range. In order to check device symmetry, measurements were performed at −30°, −50°, and −90° as well. The observed angular dependence is in agreement with the results previously reported for a similar SCDD in a clinical photon beam [20].

4. Summary and conclusions

A prototype synthetic single crystal diamond Schottky photodiode, operating at zero bias voltage, was studied and characterized as dosimeter for proton beams at the CATANA ocular proton therapy facility.

Diamond detector response was investigated in both unmodulated and modulated proton beams. A Markus plane parallel ionization chamber was used as reference for dose calibrations, an Advanced Markus chamber was used as reference for depth-dose measurements, and EBT2 radiochromic films were employed as reference for determination of output factors for narrow proton fields.

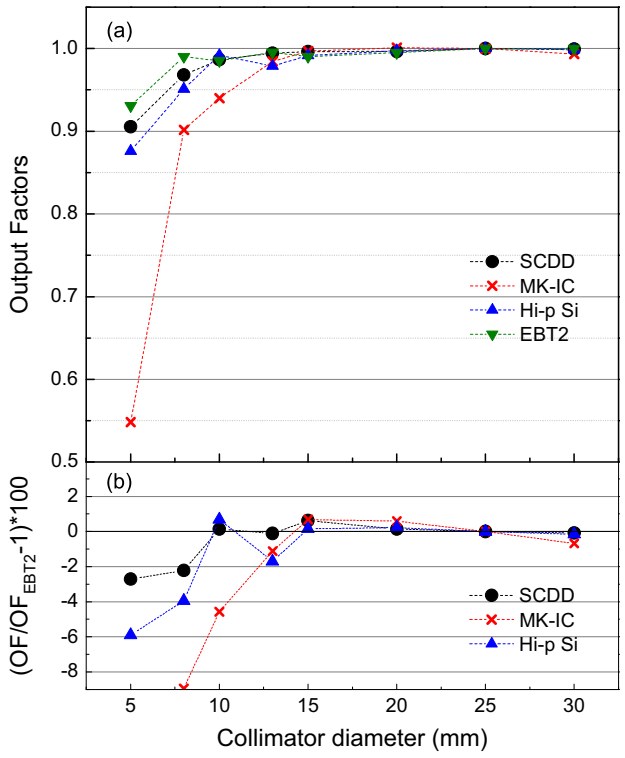

Fig. 6. (a) Output factors measured by SCDD, Markus chamber, Scanditronix Hi-p Si diode and radiochromic EBT2 as function of collimator diameter. (b) Relative differences of OFs by SCDD, MK-IC and Hi-p Si diode with respect to those measured by EBT2 films.

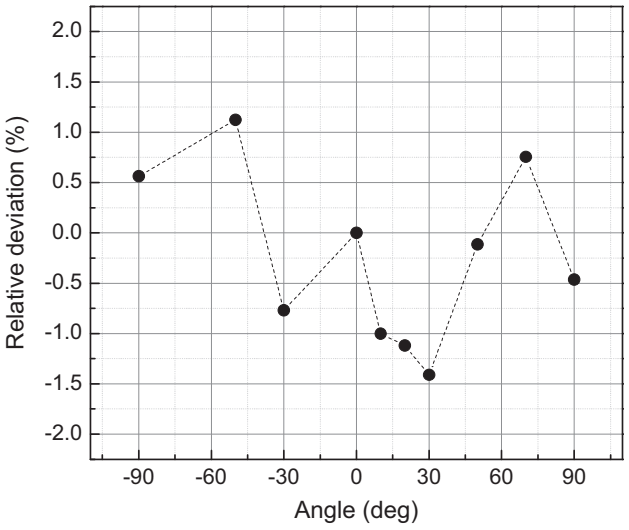

Fig. 7. Angular dependence of the SCDD response as normalized deviation to the 0° value.

The diamond dosimetric properties were studied characterizing its response with respect to the pre-irradiation dose, the absorbed dose and dose rate, the field size (OFs) and the beam incidence direction; also the suitability for depth-dose measurement was deeply investigated.

A negligible signal variation, within 0.5%, was found in the pre-irradiation procedure for the tested diamond detector. Deviations within $\pm 0.5\%$ were observed in the diamond response with dose and dose rate over the investigated ranges: 0.5–40 Gy and 0.33–30 Gy/min respectively. Output factors were measured with the SCDD detector at the calibration depth ($z_{ref.}$) and modulated proton beams with circular beam spot size of radius in varying from 5 mm to 30 mm in diameter. Responses were compared to the ones obtained from a PFD stereotactic Si diode and radiochromic EBT2 film. A good agreement was found between the OFs from SCDD detector and EBT2 film, with a maximum deviation of $\sim 3\%$ found with the smallest 5 mm in diameter circular collimator.

Depth-dose curves were measured for the unmodulated 62 MeV full energy proton beam, for three unmodulated range-shifted proton beams and for a therapeutic modulated proton beam (SOBP). Depth dose curves measured by SCDD resulted in excellent agreement with those from the reference Advanced Markus chamber, with relative differences lower than $\pm 1\%$ in peak-to-plateau ratios, well within experimental uncertainties. This indicates that the diamond response does not depend on the proton beam energy nor on the linear energy transfer. Finally, a 2.5% variation in diamond detector response was observed in angular dependence measurements by varying the proton beam incidence angle in the polar direction.

The results reported for the tested synthetic single crystal diamond detector strongly indicate its suitability for an accurate dosimetry characterization of the narrow ocular proton-therapy beams, with no need of any correction factor accounting for dose rate and linear energy transfer dependence.

Acknowledgements

This work is supported by the EMRP joint research project MetrExtRT which has received funding from the European Union on the basis of Decision No. 912/2009/EC. The EMRP is jointly funded by the EMRP participating countries within EURAMET and the European Union.

References

[1] S. Webb, The Physics Of Three-Dimensional Radiation Therapy, IOP Publishing, Bristol, UK, 1993.
[2] B. Vikram, C.N. Coleman, J.A. Deye, Oncology 23 (2009) 279.
[3] E.J. Hall, C. Wuu, International Journal of Radiation Oncology, Biology, Physics 56 (2003) 83.
[4] R.R. Wilson, Radiology 47 (1946) 487.
[5] M. Goitein, A. Lomax, E. Pedroni, Physics Today 55 (2002) 45.
[6] E. Pedroni, R. Bacher, H. Blattman, T. Böhringer, A. Coray, A. Lomax, L. Shixiong, G. Munkel, S. Scheib, U. Schneider, A. Tourosky, Medical Physics 22 (1995) 37.
[7] T. Haberer, W. Becher, D. Schardt, G. Kraft, Nuclear Instruments and Methods in Physics Research A 330 (1993) 296.
[8] ⟨http://www.ptcog.ch/index.php/facilities-in-operation⟩.
[9] ICRU (International Commission on Radiation Units and Measurements), Prescribing, Recording, and Reporting Proton-Beam Therapy, ICRU Report No. 78 (International Commission on Radiation Units and Measurements, Bethesda, MD; 2008).
[10] IAEA (International Atomic Energy Agency), Absorbed dose determination in external beam radiotherapy: an international code of practice for dosimetry based on standards of absorbed dose to water, Technical Report Series No. 398, IAEA, Vienna, 2000.
[11] C.P. Karger, O. Jäkel, H. Palmans, T. Kanai, Physics in Medicine & Biology 55 (2010) 193.
[12] E. Grusell, J. Medin, Physics in Medicine & Biology 45 (2000) 2573.
[13] M. Pacilio, C. De Angelis, S. Onori, L. Azario, A. Fidanzio, R. Miceli, A. Piermattei, A. Kacperek, Physics in Medicine & Biology 47 (2002) 107.
[14] S. Onori, C. De Angelis, P. Fattibene, M. Pacilio, E. Petetti, L. Azario, R. Miceli, A. Piermattei, L. Barone Tonghi, G. Cuttone, S. Lo Nigro, Physics in Medicine & Biology 45 (2000) 3045.
[15] G.A.P. Cirrone, G. Cuttone, S. Lo Nigro, V. Mongelli, L. Raffaele, M.G. Sabini, L. Valastro, M. Bucciolini, S. Onori, Nuclear Instruments and Methods in Physics Research A 552 (2005) 197.
[16] A. Fidanzio, L. Azario, C. De Angelis, M. Pacilio, S. Onori, A. Kacperek, A. Piermattei, Medical Physics 29 (2002) 669.
[17] U. Sowa, T. Nowak, B. Michalec, G. Mierzwińska, J. Swakoń, P. Olko, Nukleonika 57 (2012) 491.
[18] A.K. Mandapaka, A. Ghebremedhin, B. Patyal, Marco Marinelli, G. Prestopino, C. Verona, G. Verona-Rinati (121702-1), Medical Physics 40 (2013).
[19] ICRU (International Commission on Radiation Units and Measurements), Clinical Proton Dosimetry: Part I. Beam Production, Beam Delivery and Measurement of Absorbed Dose, ICRU Report No. 59 (International Commission on Radiation Units and Measurements, Bethesda, MD; 1998).
[20] I. Ciancaglioni, Marco Marinelli, E. Milani, G. Prestopino, C. Verona, G. Verona-Rinati, R. Consorti, A. Petrucci, F. De Notaristefani, Medical Physics 39 (2012) 4493.

[21] C. Di Venanzio, Marco Marinelli, E. Milani, G. Prestopino, C. Verona, G. Verona-Rinati, M.D. Falco, P. Bagalà, R. Santoni, M. Pimpinella (021712-1), Medical Physics 40 (2013).
[22] P. Bagalà, C. Di Venanzio, M.D. Falco, A.S. Guerra, Marco Marinelli, E. Milani, M. Pimpinella, F. Pompili, G. Prestopino, R. Santoni, A. Tonnetti, C. Verona, G. Verona-Rinati, Physics in Medicine & Biology 58 (2013) 8121.
[23] G.A.P. Cirrone, G. Cuttone, P.A. Lojacono, S. Lo Nigro, V. Mongelli, I.V. Patti, et al., IEEE Transactions on Nuclear Science NS51 (2004) 860.
[24] N. Givehchi, F. Marchettoemail, L.M. Valastro, A. Ansarinejad, A. Attili, M.A. Garella, S. Giordanengo, V. Monaco, J. Pardo Montero, R. Sacchi, A. Boriano, F. Bourhaleb, R. Cirio, A. La Rosa, A. Pecka, C. Peroni, G.A.P. Cirrone, G. Cuttone, M. Donetti, S. Iliescu, S. Pittera, L. Raffaele, Physica Medica 27 (2011) 233.
[25] G. Cuttone, G.A.P. Cirrone, G. Di Franco, V. La Monaca, S. Lo Nigro, J. Ott, S. Pittera, G. Privitera, L. Raffaele, A. Reibaldi, F. Romano, M.G. Sabini, V. Salamone, M. Sanfilippo, C. Spatola, L.M. Valastro, The European Physical Journal Plus 65 (2011) 126.
[26] S. Almaviva, M. Marinelli, E. Milani, G. Prestopino, A. Tucciarone, C. Verona, G. Verona-Rinati, M. Angelone, M. Pillon, I. Dolbnya, K. Sawhney, N. Tartoni, Journal of Applied Physics 107 (2010) 014511.
[27] L. Zhao, I.J. Das, Gafchromic, Physics in Medicine & Biology 55 (2010) 291.
[28] S.N. Rustgi, M.D.F. Douglas, Medical Physics 22 (1995) 2117.
[29] W.U. Laub, T.W. Kaulich, F. Nusslin, Physics in Medicine & Biology 44 (1999) 2183.
[30] J.F. Fowler, F.H. Attix, Solid state electrical conductivity dosimeters (Chapter14), in: F.H. Attix, W.C. Roesch (Eds.), Radiation Dosimetry, 2nd ed., AcademicPress, New York, 1966.
[31] D. Kirby, S. Green, H. Palmans, R. Hugtenburg, C. Wojnecki, D. Parker, Physics in Medicine & Biology 55 (2010) 417.